Tellus (1984), *36A*, 187–202

A model study of downstream variations of the thermodynamic structure of the trade winds

By BRUCE A. ALBRECHT[1], *National Center for Atmospheric Research*[2], *Boulder, Colorado 80307, USA*

(Manuscript received May 3, 1982; in final form May 10, 1983)

ABSTRACT

A simple model is used to study downstream variations in the thermodynamic structure of the trade-wind boundary layer due to downstream variations in sea-surface temperature, divergence, surface wind speed, and the thermodynamic structure above the inversion. Model results indicate that dry and cold air advection due to an equatorward increase in sea-surface temperature results in a boundary layer that is less than 1 °C cooler and 1 g kg^{-1} drier than that obtained for steady-state horizontally homogeneous conditions. Although the magnitude of the advection terms in the heat and moisture budgets may be relatively large, below the inversion they are generally balanced by increased convective heating and moistening. The downstream variations in the temperatures below the inversion are relatively insensitive to variations in any of the external parameters and were generally within 1 °C of the homogeneous solutions. The mixing ratio, however, is sensitive to variations in the surface wind speed and the thermodynamic structure above the inversion.

The height of the trade inversion obtained for the various downstream experiments was found to differ significantly from the horizontally homogeneous solutions. These differences indicate that the height of the inversion may depend more on upstream rather than local conditions. The downstream variations in the inversion height depend on sea-surface temperature, divergence, variations in the temperature and moisture above the inversion, surface wind speeds, and radiative cooling variations.

1. Introduction

An imporant feature of the earth's general circulation is the equatorward flow of air associated with the trades. As the trades flow equatorward they accumulate latent and sensible heat. As shown by Riehl and Malkus (1957), the heat exported in this process provides energy for the maintenance of the Hadley circulation. The downstream variation in the thermodynamic structure of the Pacific trades was clearly described by Riehl et al. (1951). They used data obtained along a line from San Francisco to Hawaii and showed an increase in the temperature and moisture of the boundary layer and an increase in the height of the trade inversion along this line.

Some general aspects of the downstream variation in the trades have been studied theoretically by Malkus (1956), Mak (1976), and Ogura (1977). They used models which considered the trade flow to be two-dimensional and used linearized governing equations to demonstrate some of the qualitative features of the trade flow, including the steadiness of the flow and downstream variations in the height of the trade inversion. The results from these models demonstrated the role of convective processes in maintaining the heating needed to drive the circulation. The heating in the studies described above was specified externally, although as Malkus (1956) pointed out, the convective and small-scale processes may actually regulate the large-scale flow.

[1] Permanent affiliation: The Pennsylvania State University, University Park, Pennsylvania 16802.

[2] The National Center for Atmospheric Research is sponsored by the National Science Foundation.

Convective processes in the trades help maintain the characteristic thermodynamic structure of the trades. The most notable feature of this structure is the trade inversion. Riehl et al. (1951), noted that the evaporation of cloud water at the trade inversion produces cooling and moistening which help balance the large-scale subsidence warming and drying. Convective processes in the cloud layer help keep this layer conditionally unstable in spite of the stabilization due to subsidence (Betts, 1973).

Heat and moisture budget studies, such as those made by Augstein et al. (1973), Holland and Rasmusson (1973), and Nitta and Esbensen (1974), used observations to estimate the role of convective processes in the maintenance of the thermodynamic structure of the trades. Betts (1975) used fluxes obtained from a budget study to show how the convective effects may be interpreted in terms of detrainment moistening and cooling and cumulus induced subsidence warming and drying. Aircraft measurements such as those described by LeMone and Pennell (1976) and Nicholls and LeMone (1980) have helped define the subcloud layer processes in the trades.

The observational studies of the trade-wind boundary layer provided considerable guidance for the development of a model described by Albrecht et al. (1979, hereafter referred to as A79). This model predicts the height of the trade inversion and the thermodynamic structure below it, where wind speed, large-scale divergence and sea-surface temperature are specified externally. A similar model with a more explicit cumulus parameterization scheme is described by Augstein and Wendel (1980).

In this study the A79 model is used to study the downstream variations in the trade-wind boundary layer due to variations in sea-surface temperature, large-scale divergence, surface wind speeds and the thermodynamic structure above the inversion. The downstream variations in the large-scale boundary conditions are specified externally and simulate the variation of these conditions along a trajectory. Schubert et al. (1979) and Kraus and Leslie (1982) used a cloud-topped mixed-layer model similar to that described by Lilly (1969) to study downstream variations in boundary layers associated with stratocumulus. Kraus and Leslie (1982) also considered the downstream variations in ocean surface conditions using a mixed layer ocean model in conjunction with the stratocumulus model.

2. Description of the model

The model described in A79 represents the trade-wind boundary layer as the idealized structure shown in Fig. 1. The vertical coordinate used in the model is $\hat{p} = p_0 - p$ where p_0 is the surface pressure. The variables used to represent the structure shown in Fig. 1 are mixing ratio q and dry static energy $s = c_p T + gz$ where c_p is the specific heat of air at constant pressure, T is Kelvin temperature and g is the acceleration due to gravity. The idealized structure consists of a cloud layer and a subcloud layer separated by a transition layer of infinitesimal thickness at $\hat{p}_B$, and the cloud layer is capped by an infinitesimally thin trade inversion layer at $\hat{p}_I$. In the subcloud layer it is assumed that mixing ratio and dry static energy are constant with pressure and represented as q_M and s_M. In the cloud layer these quantities are represented as linear functions of pressure so that $s = s_A + \gamma_s p'$ and $q = q_A + \gamma_q p'$ where $p' = \hat{p} - (\hat{p}_B + \hat{p}_I)/2$, the subscript A refers to the layer average, and γ_q and γ_s are the slopes of q and s. The thermodynamic profiles above the inversion are specified externally or from a large-scale model.

The structure of the model is the area-averaged structure of the boundary layer. It is assumed that the area considered is large enough to include many non-precipitating cumuli. Thus convective processes are assumed to be sub-grid scale and are parameterized as a function of the large-scale fields.

2.1. *Governing equations*

The boundary layer structure described above is represented by the eight variables s_M, q_M, s_A, γ_s, γ_q, $\hat{p}_B$, and $\hat{p}_I$. Area-averaged heat and moisture budget equations are used to formulate the predictive equations for the variables described above. These equations express changes in the structure due to radiative, convective and large-scale processes. Vertical velocity is specified in this model as a linear function of the form $\omega = -D\hat{p}$ where D is the mean divergence and $\omega \equiv \mathrm{d}\hat{p}/\mathrm{d}t$.

The results presented by Riehl et al. (1951) show that there is little vertical wind shear below the trade inversion. Assuming no vertical wind shear, allows one to consider the variations in the boundary layer structure along a horizontal trajectory. Following A79, the equations describing the variation of the thermodynamic structure shown in Fig. 1 may be written in a natural coordinate system as

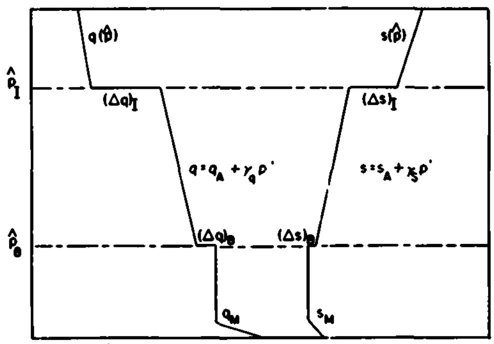

Fig. 1. Idealized boundary layer structure assumed in the model.

$$\frac{\partial s_M}{\partial t} + V\frac{\partial s_M}{\partial x} = -g[(F_s)_{B-} - (F_s)_0]/\hat{p}_B + Q_{RM} \quad (1)$$

$$\frac{\partial q_M}{\partial t} + V\frac{\partial q_M}{\partial x} = -g[(F_q)_{B-} - (F_q)_0]/\hat{p}_B \quad (2)$$

$$\frac{\partial s_A}{\partial t} + V\frac{\partial s_A}{\partial x} = \gamma_s\left(\frac{\partial \hat{p}_A}{\partial t} + \frac{\partial \hat{p}_A}{\partial x} - \hat{\omega}_A\right)$$
$$-g[(F_{sl})_{I-} - (F_{sl})_{B+}]/\delta\hat{p} + Q_{RA} \quad (3)$$

$$\frac{\partial q_A}{\partial t} + V\frac{\partial q_A}{\partial x} = \gamma_q\left(\frac{\partial \hat{p}_A}{\partial t} + V\frac{\partial \hat{p}_A}{\partial x} - \hat{\omega}_A\right)$$
$$-g[(F_{q+l})_{I-} - (F_{q+l})_{B+}]/\delta\hat{p} \quad (4)$$

$$\frac{\partial \gamma_s}{\partial t} + V\frac{\partial \gamma_s}{\partial x} = D\gamma_s - 4g[(F_{sl})_{I-} - 2(F_{sl})_A$$
$$+ (F_{sl})_{B+}]/(\delta\hat{p})^2 + \left(\frac{\partial Q_R}{\partial \hat{p}}\right)_A \quad (5)$$

$$\frac{\partial \gamma_q}{\partial t} + V\frac{\partial \gamma_q}{\partial x} = D\gamma_q - 4g[(F_{q+l})_{I-} - 2(F_{q+l})_A$$
$$+ (F_{q+l})_{B+}]/(\delta\hat{p})^2 \quad (6)$$

$$\frac{\partial \hat{p}_B}{\partial t} + V\frac{\partial \hat{p}_B}{\partial x} = -D\hat{p}_B + g[(F_{sl})_{B+} - (F_s)_{B-}]/(\Delta s)_B \quad (7)$$

$$\frac{\partial \hat{p}_I}{\partial t} + V\frac{\partial \hat{p}_I}{\partial x} = -D\hat{p}_I - g\frac{(F_{sl})_{I-}}{(\Delta s)_I} + g\frac{\Delta F_R}{(\Delta s)_I} \quad (8)$$

where V is the wind speed and x is the distance along the trajectory, $\delta\hat{p} = \hat{p}_I - \hat{p}_B$, Q_{RM} is the radiative heating rate averaged over the depth of the mixed layer, Q_{RA} is the radiative heating rate averaged over the depth of the cloud layer. The $(\partial Q_R/\partial p)_A$ term represents the vertical variation of the radiative heating averaged over the depth of the cloud layer, and ΔF_R is a radiative flux divergence across the trade inversion which simulates cooling in the trade inversion due to cloud top cooling; F_s, F_q, F_{sl} and F_{q+l} refer to convective fluxes of the quantities s, q, $s - Ll$ and $q + l$ respectively where l is the liquid water mixing ratio. The subscripts 0, B, A, and I in (1)–(8) refer to the various pressure levels defined above and in Fig. 1. The jumps $(\Delta s)_I$, $(\Delta q)_I$, $(\Delta s)_B$, and $(\Delta q)_B$ are shown in Fig. 1 and defined as $(\Delta s)_I \equiv s(\hat{p}_{I+}) - s(\hat{p}_{I-})$, $(\Delta q)_I \equiv q(\hat{p}_{I+}) - q(\hat{p}_{I-})$, $(\Delta s)_B \equiv s(\hat{p}_{B+}) - s_M$, $(\Delta q)_B \equiv q(\hat{p}_{B+}) - q_M$. The $\partial\hat{p}_A/\partial t + V\,\partial\hat{p}_A/\partial x$ term in eqs. (3) and (4) can be expressed as a function of the convective and radiative fluxes using eqs. (7) and (8) since $\hat{p}_A = (\hat{p}_B + \hat{p}_I)/2$. Eqs. (1)–(8) are equivalent to the A79 equations except for the addition of the $V\,\partial/\partial x$ terms.

The left-hand side of the predictive equation may be considered as total derivatives and these equations may be solved numerically provided the various terms on the right side can be expressed as a function of the independent and dependent variables or externally specified parameters. For horizontally homogeneous conditions, the $V\,\partial/\partial x$ terms are zero and the solutions obtained with (1)–(8) give the local time variations. Alternately, eqs. (1)–(8) may be integrated to give solutions along a trajectory using x as the independent variable.

In this study the model is used in its downstream mode to study how downstream variations in various large-scale parameters affect the evolution of the trade-wind boundary layer.

2.2. *Closure assumptions*

Given below is a brief description of the closure needed to solve the predictive equations above. Details of the parameterization and the sensitivity of the steady-state solutions to the closure assumptions and large-scale variables are given in A79 and Albrecht (1979).

Surface fluxes of sensible and latent heat are specified using bulk aerodynamic formulas as

$$(F_s)_0 = \rho C_T V(s_0 - s_M) \quad (9)$$

and

$$(F_q)_0 = \rho C_q V(q_0 - q_M) \quad (10)$$

where ρ is density, $s_0 = c_p T_0$ where T_0 is sea-surface temperature and q_0 is the saturation mixing ratio of air at temperature T_0. The coefficients C_T and C_q are bulk transfer coefficients and are specified as constants with a value of 1.15 × 10^{-3}. The value used for these coefficients is slightly reduced from that used when (9) and (10) are applied at 10 m heights since s_M and q_M are values above the surface layer.

Fluxes at the top of the subcloud or mixed layer are specified using the mixed layer closure of assuming that the virtual dry static energy flux F_{sv} (where $s_v = c_p T_v + gz$ and T is virtual temperature) at the top of the mixed layer is some negative fraction of the virtual static energy flux at the surface so that $(F_{sv})_{B-} = -k(F_{sv})_0$. This assumption has been used extensively in dry mixed layer models (e.g., Stull, 1976). The validity of this closure for a layer capped by shallow cumulus clouds has been demonstrated by LeMone and Pennell (1976) and Nicholls and LeMone (1980). For the results shown here $k = 0.20$, a value consistent with the values obtained from observations.

Cloud layer fluxes are formulated using a simple cumulus parameterization scheme. The convective fluxes are parameterized as a product of a cloud mass flux ω^* and cloud-environment differences in thermodynamic variables, where the clouds are assumed to be nonprecipitating. This type of representation of the fluxes is discussed by Betts (1975) and may be used to write

$$F_{sl} = \frac{\omega^*}{g}[s_c - Ll_c - \bar{s}] \tag{11}$$

$$F_{q+l} = \frac{\omega^*}{g}[q_c + l_c - \bar{q}] \tag{12}$$

where the subscript c refers to in-cloud values and s and q are mean values and are given by the model structure described above.

The parameterization given by (11) and (12) represents the fluxes using a single cloud type. In reality there may be clouds in the boundary layer which have tops at various heights. Betts (1975), however, used BOMEX data to show that the use of a single cloud-type gives a satisfactory representation of fluxes in the undisturbed boundary layer.

To obtain the fluxes given by (11) and (12), the mass flux and the in-cloud values need to be parameterized as functions of the thermodynamic structure of the model. Since the cloud layer structure is specified to be linear with $\hat{p}$, the fluxes given by (11) and (12) may be constrained to be no more than quadratic with $\hat{p}$. This quadratic dependence is obtained by assuming a linear cloud-environment difference in thermodynamic variables and a linear mass flux distribution. Thus the product of these quantities is a quadratic function of $\hat{p}$.

The cloud properties are defined using entrainment relationships of the form

$$\frac{\partial(s_c - Ll_c)}{\partial \hat{p}} = -\frac{E}{\delta p}(s_c - Ll_c - \bar{s}) \tag{13}$$

$$\frac{\partial(q_c + l_c)}{\partial \hat{p}} = -\frac{E}{\delta p}(q_c + l_c - \bar{q}) \tag{14}$$

where E is an entrainment parameter. These equations will, with appropriate boundary conditions, give the in-cloud values as functions of the area-averaged model structure. Eqs. (13) and (14) may be solved analytically since s and q in the model are linear functions of $\hat{p}$. It is also assumed that at cloud base, clouds have the thermodynamic characteristics of the subcloud layer. The solutions obtained from (13) and (14) are then linearized as in A79.

The entrainment parameter E is obtained by assuming that the cloud-environment difference in virtual dry static energy averaged over the depth of the cloud is some fraction of that obtained with no entrainment. This may be written as

$$\frac{1}{c_p \delta \hat{p}} \int_0^{\hat{p}} (s_{vc} - \bar{s}) \mathrm{d}\hat{p} = \alpha \, \Delta T_{vc} \tag{15}$$

where ΔT_{vc} is the cloud-environment differences in virtual temperature averaged over the cloud layer with $E = 0$ and $0 \leq \alpha \leq 1$.

The closure assumption given by (15) ensures that the clouds parameterized in the model experience a positive bouyancy force averaged over the depth of the cloud layer. While there may be individual clouds that satisfy the extreme conditions of $\alpha = 0$ and $\alpha = 1$, the average cloud would most likely have a value somewhere between these extremes. For the results presented here, a value of $\alpha = 0.5$ is assumed. While it may be possible to obtain a better estimate of α from three-dimensional model results such as those presented by Sommeria (1976), sensitivity tests shown below indicate that the downstream solutions are insensitive to the value of α.

The linear variation of the cloud mass flux is represented as

$$\omega^* = \omega_B^*[1 + \mu(\hat{p} - \hat{p}_B)], \quad \hat{p}_B \le \hat{p} \le \hat{p}_I$$
$$\omega^* = 0, \quad \hat{p} > \hat{p}_I \tag{16}$$

where ω_B^* is the mass flux at cloud base.

The cloud base mass flux ω_B^* is obtained by assuming that the lifting condensation level (LCL) of air in the mixed layer is at the transition layer, level $\hat{p}_B$. This parameterization was proposed by Betts (1973). Fitzjarrald and Garstang (1981) used high resolution soundings in the tropical Atlantic to show that, for average conditions, assuming the LCL to be at the top of the mixed layer is reasonable. This assumption allows (7) to be combined with (1) and (2) to determine $(F_{sl})_{B+}$, and hence ω_B^*, since $\omega_B^* = -(F_{sl})_{B+}/(\Delta s)_B$.

The vertical variation of the mass flux in (16) is parameterized using the expression for μ derived in A79 as

$$\mu = \frac{E}{\delta\hat{p}} - \frac{1}{2\omega_B^* \tau_a}(1 + 2/3\, E) \tag{17}$$

where E is the entrainment factor and τ_a is a time scale which is specified as a constant. This time scale specifies the rate at which cloud matter detrains in the cloud layer and similar detrainment rates have been discussed by Fraedrich (1973), Betts (1976), Cho (1977), and A79. The representation of the vertical variation of the mass flux given by (17) is based on the simple transient cloud model described by Betts (1975) and A79. An estimate of $\tau_a = 1/3$ day was also obtained from the Betts (1976) analysis, which is based on data collected during the Barbados Meteorological and Oceanographic Experiment, 1979. Eq. (16) also simulates the detrainment of cloud mass at the trade inversion due to the discontinuity in the mass flux.

Eqs. (9)–(17) are used to obtain the convective fluxes in the predictive equations as a function of the mean fields. The sensitivity of the downstream solutions to the closure parameters τ_a, α, and k is presented below.

The radiative fluxes in the trade-wind boundary layer may have a complex interaction with the fractional coverage of clouds and their height distribution since the model equations apply to an area that includes both clear and cloudy regions. In A79 longwave radiative flux calculations were made for both clear and cloudy atmospheres. They showed that the cooling averaged over the depth of the boundary layer was approximately the same for the clear and the cloudy conditions when temperature and moisture profiles typical of the trades were assumed. In the cloud case, however, the cooling is confined to a thin layer at the top of the cloud, while for clear-sky conditions, the cooling is more uniformly distributed in the vertical.

If the cloud-top heights are uniformly distributed over the depth of the cloud layer, the large-scale cooling associated with the clouds would also be uniformly distributed in the vertical. In the trades, however, the inversion is significantly more stable than the cloud layer and represents an upper limit on the cloud top heights. Consequently, there is a maximum in the cloud-top cooling at the inversion. This cooling is represented as the flux divergence, ΔF_R, in the equation which predicts the height of the inversion.

For the results presented here it is assumed that 50% of the average boundary layer cooling occurs in the inversion and 50% occurs below it. The net boundary layer cooling is assumed to be a constant 3 °C/day^{-1}, which is consistent with the value calculated by A79. These assumptions give $Q_{RM}/c_p = Q_{RA}/c_p = Q_R/c_p = -1.5$ °C/day^{-1}, $\Delta F_R = \hat{p}_I Q_R/g$, and $(\partial Q_R/\partial\hat{p})_A = 0$.

The radiative cooling in the real atmosphere may be more complicated than that assumed in the model. Cloud cover, for example, may vary along a trajectory since it is a function of the boundary layer structure (Albrecht, 1981). However, to isolate the effects due to downstream variations in the boundary conditions, constant radiative cooling is assumed and no feedback between cloud formation and the radiative heating is considered. Sensitivity of the downstream variations to the assumed cooling was determined and these results are discussed below.

The thermodynamic structure above the inversion is specified externally as a linear function of $\hat{p}$ so that

$$q(\hat{p}) = q_{00} + \Gamma_q \hat{p} \tag{18}$$

and

$$s(\hat{p}) = s_{00} + \Gamma_s \hat{p} \tag{19}$$

Values for q_{00}, s_{00}, Γ_s, and Γ_q were chosen to be consistent with the structure observed during ATEX (Augstein et al., 1973). A summary of the values assigned to these variables, as well as values of other specified parameters needed in the model are summarized in Table 1. Although T_0, V, D, and the thermodynamic profiles above the inversion can be a function of x, when they are held constant they have the values given in Table 1.

The closure outlined in (9)–(19) allows the right-hand side of (1)–(8) to be expressed as functions of the model structure and various externally specified parameters. A Runge–Kutta fourth-order method is used with a 500 s time step (or ~4 km space step) to integrate (1)–(8). The convective flux $(F_{q+1})_{I-}$ given by eq. (12) is adjusted slightly following the procedure given by A79. This adjustment ensures that the fluxes at the inversion are consistent with the assumption that the moisture and temperature discontinuities are maintained at the same level $\hat{p}_I$. Without this adjustment, moisture can be fictitiously lost or created in the model.

3. Model results

The model described above is used to study the effect that downstream variations in external conditions have on the thermodynamic structure of the trades. The model is initialized by assuming horizontally homogeneous conditons (terms involving $V\,\partial/\partial x$ are zero) and integrating (1)–(8) until the solution becomes steady. The downstream integration is then performed by starting from this steady-state solution and varying external conditions in the downstream direction.

In all the results presented, the horizontal variations in sea-surface temperature and divergence are assumed to be linear with distance so that

$$T_0 = T_I + \beta_T x \tag{20}$$

$$D = D_I + \beta_D x \tag{21}$$

where T_I and D_I are the sea-surface temperature and divergence values at $x = 0$. The β_T and β_D terms in (20) and (21) specify the gradients of the temperature and the divergence.

3.1. *Sensitivity to closure assumptions*

The sensitivity of downstream variations to the cloud parameterization closure assumptions as evaluated with a $\beta_T = 2\,°\mathrm{C}/1000$ km and $\beta_D = -2 \times 10^{-6}\ \mathrm{s^{-1}}/1000$ km solution. A reference solution was obtained using the values of k, α, and τ_a, given in Table 1, and $T_I = 22\,°\mathrm{C}$ and $D_I = 5 \times 10^{-6}\ \mathrm{s^{-1}}$. The difference between the model structure at $x =$ 2000 km and $x = 0$ was evaluated and that difference was compared to the downstream differences obtained with different values of the closure parameters. These results are shown in Table 2 and show the uncertainty in the downstream variation due to uncertainties in the closure parameters.

Downstream differences were obtained with (i) $k = 0.3$, $\alpha = 0.5$, $\tau_a = 0.33$; (ii) $k = 0.2$, $\alpha = 0.25$, $\tau_a = 0.33$; and (iii) $k = 0.2$, $\alpha = 0.50$, $\tau_a = 0.25$ day and compared to the reference solution. The

Table 1. *Summary of physical parameters and closure parameters specified externally in the model*

Physical parameters	Closure parameters
$T_0 = 25\,°\mathrm{C}$	$k = 0.20$
$V = 8\ \mathrm{m\,s^{-1}}$	$C_T = 1.15 \times 10^{-3}$
$D = 5 \times 10^{-6}\ \mathrm{s^{-1}}$	$\tau_a = 1/3$ day
$s_{00} = 300.0\ \mathrm{kJ\,kg^{-1}}$	$\alpha = 0.5$
$q_{00} = 8.0\ \mathrm{g\,kg^{-1}}$	
$\Gamma_s = 4.67 \times 10^{-2}\ \mathrm{kJ\,kg^{-1}\,mb^{-1}}$	
$\Gamma_q = 1.43 \times 10^{-2}\ \mathrm{g\,kg^{-1}\,mb^{-1}}$	

Table 2. *Differences between the downstream variations for solutions obtained with the values of k, α, and τ_a listed and the reference case which uses the k, α, and τ_a values given in Table 1. For these results β_T = 2 °C (1000 km)$^{-1}$ and γ_D = −2 × 10^{-6} s^{-1} (1000 km)$^{-1}$. The variations compared are for a downstream distance of 2000 km*

	$k = 0.3$ (−ref)	$\tau_a = 1/4$ day (−ref)	$\alpha = 0.25$ (−ref)
q_M (g kg^{-1})	−0.11	0.02	0.02
s_M (kJ kg^{-1})	0.05	0.00	0.00
p_B (mb)	2.5	−0.50	−0.40
q_A (g kg^{-1})	−0.05	−0.10	−0.06
s_A (kJ kg^{-1})	0.07	0.06	0.050
γ_q (g/kg/mb)	0.0004	−0.0004	0.0010
γ_s (kJ/kg/mb)	−0.0001	0.0001	−0.0004
P_I (mb)	2.90	1.30	1.00

downstream variation of the structure of the boundary layer for these three cases differs little from the reference case and below the inversion these differences are generally less than 0.1 g/kg and 0.05 °C. Downstream variations in the slopes of q and s in the cloud layer are also relatively insensitive to the values of the closure parameters. Uncertainties in the downstream variation of the inversion height and the mixed layer height are less than 3 mb for the cases considered. The initial conditions obtained from the horizontally homogeneous conditions are also relatively insensitive to the closure parameters, which is consistent with the A79 steady-state results.

3.2. *Sea-surface temperature variations*

Parcels near the surface which move equatorward with the trades generally move over increasingly warmer sea-surface temperatures and experience decreasing large-scale divergence. The effect of a downstream increase in sea-surface temperature was evaluated by specifying T_0 = 22 °C and β_T = 2 and 4 °C (1000 km)$^{-1}$. The downstream variations in the height of the transition layer and the trade inversion for these calculations are shown in Fig. 2. For both sea-surface temperature gradients, the depth of the cloud layer increases only slightly as both cloud base and the height of the trade inversion increase in the downstream direction. These results are consistent with the steady-state results shown in A79, where variations in sea-surface temperature result in variations in the mean height of the layer with little change in the thickness of the cloud layer.

The downstream variation of the structure below the inversion for β_T = 2 °C (1000 km)$^{-1}$ is shown in Fig. 3. Since the LCL is assumed to be at the transition layer, the mixed layer values of q and s vary in a way which, by definition, must be consistent with variations in the height of the transition layer. The mixing ratio increases slowly in the downstream direction, while changes in the dry static energy roughly follow changes in the sea-surface temperature. As a result, the LCL increases in the downstream direction. The relatively small variation in q_M results in a downstream increase in the air–sea difference in mixing ratio. This increase in the surface moisture flux results in a greater moisture flux convergence at the trade inversion and a corresponding increase in its height. The downstream increase in the

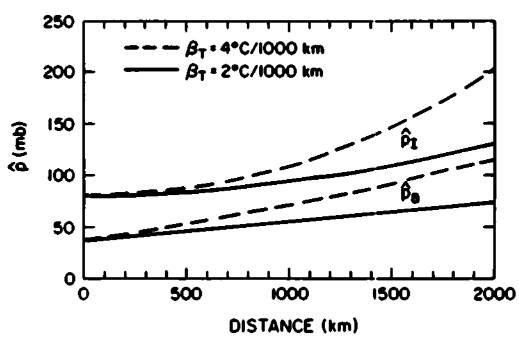

Fig. 2. Downstream variations in the height of the trade inversion for sea-surface temperature gradients of 2 °C/1000 km and 4 °C/1000 km.

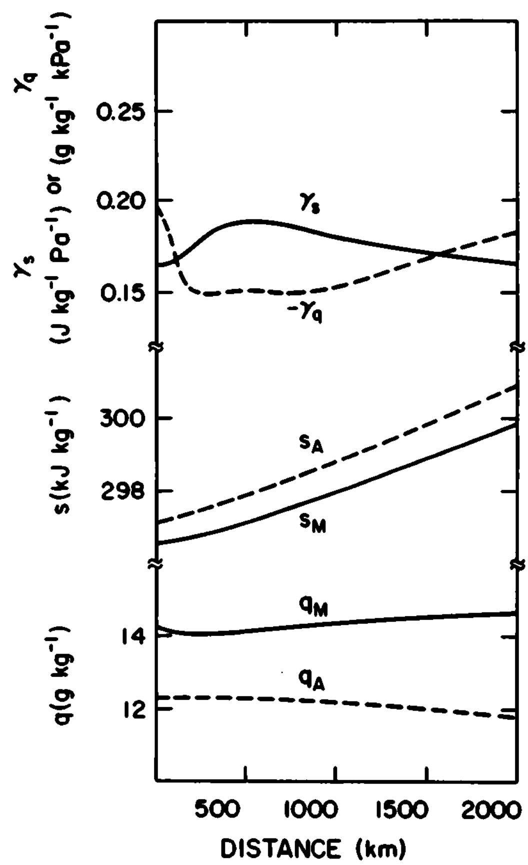

Fig. 3. Downstream variations in the thermodynamic structure below the inversion for a sea-surface temperature gradient of 2 °C/1000 km.

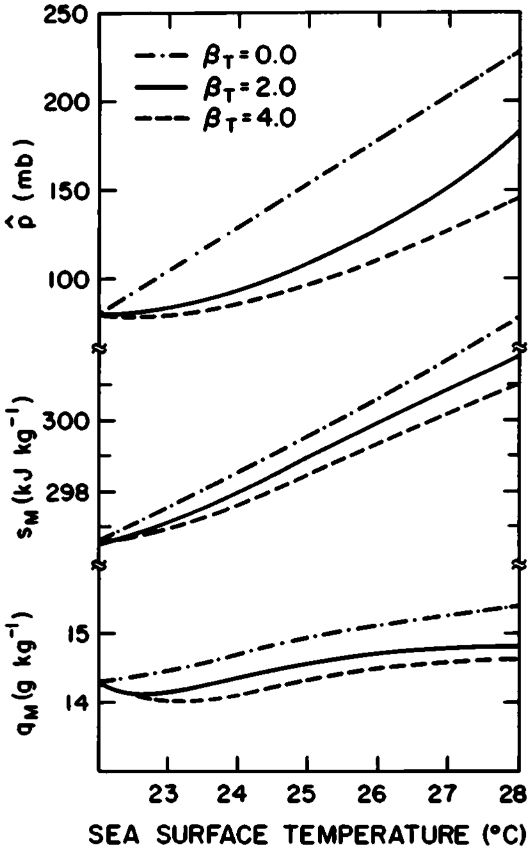

Fig. 4. Comparison of inversion height, mixed layer s and mixed layer q for horizontally homogeneous conditions, $\partial T_0/\partial x$ = 2 °C/1000 km and $\partial T_0/\partial x$ = 4 °C/1000 km.

air–sea difference in mixing ratio is consistent with the results of Riehl et al. (1951) and those shown by Hastenrath and Lamb (1977).

The variations in the cloud layer average dry static energy s_A closely follow variations in s_M; while q_A, the cloud layer mixing ratio, decreases slightly in the downstream direction. The decrease in the cloud layer mixing ratio occurs mainly in the upper part of the cloud layer as the slope of q becomes more negative in the downstream direction. The variations in γ_s and γ_q both result in a slight destabilization of the cloud layer in the downstream direction if virtual effects are considered.

The effect of advection on the boundary layer structure was evaluated by comparing the downstream solution at a given temperature with the corresponding steady-state solution. This comparison is shown in Fig. 4 for the β_T = 2 and 4 °C (1000 km)$^{-1}$ cases discussed above. The advective case is clearly cooler and drier than the corresponding horizontally homogeneous case and the depth of the boundary layer is reduced. Although the differences between the downstream and horizontally homogeneous values of q_M and s_M are relatively small, the inversion height is substantially altered by advection.

The relative role of advection is illustrated by comparing the heat and moisture budgets for the horizontally homogeneous and the downstream solutions. These budgets are shown in Table 3 for solutions obtained at a sea-surface temperature of 26 °C. The β_T = 2 °C/1000 km downstream solution is used for the inhomogeneous case.

Without advection the steady-state heat budget for the mixed layer shows a simple balance between radiative cooling and the convective warming due to the convergence of the heat flux. Because of the mixed layer assumption, changes in the heat budget due to vertical advection are zero. In the inhomogeneous case, cooling due to horizontal advection is of the same magnitude as the radiative cooling. The advective cooling is balanced by an increased convergence of the heat flux. This warming is partially maintained by an increase in the surface heat flux due to an increase in air–sea temperature differences.

In the cloud layer there is warming due to large-scale subsidence. In this layer, subsidence warming and convective heating balance the radiative cooling in the horizontally homogeneous case. For the horizontally inhomogeneous case, the cooling due to advection is balanced by an increased convective heating, since the radiative cooling and the subsidence warming are approximately the same as in the homogeneous case.

The moisture balances are somewhat simpler since there are no radiative effects. For the steady-state homogeneous case there is no divergence of the moisture flux in the mixed layer. For the horizontally inhomogeneous case the advective term causes slight drying that is balanced by a convective flux convergence. The small contribution of advection is consistent with the small horizontal gradient of q shown in Fig. 3.

In the cloud layer, the drying due to the subsidence is balanced by a convergence of the total water flux. In the advective case, the contri-

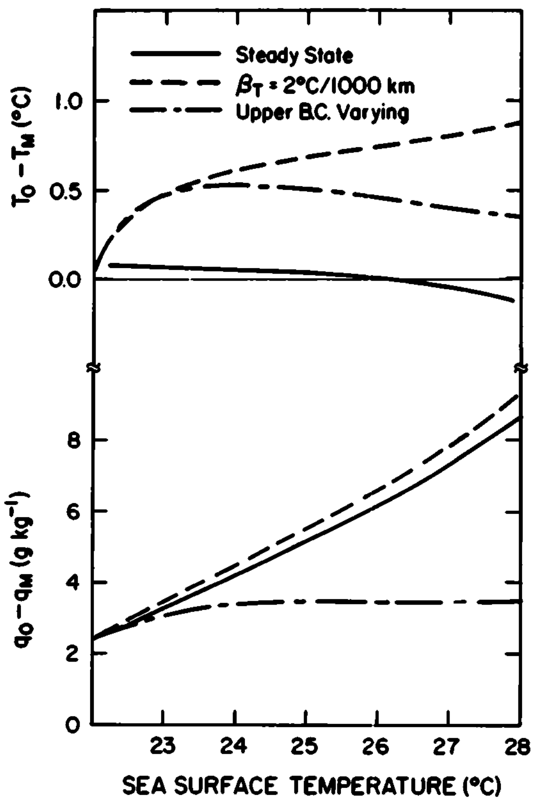

Fig. 5. Comparison of air–sea temperature and mixing ratio differences as a function of sea-surface temperature for $\partial T_0/\partial x = 2$ °C/1000 km, $\partial T_0/\partial x = 0$, and with upper boundary conditions varying.

bution of the horizontal advection is small, as it was in the subcloud layer.

The terms in the rate equation for $\hat{p}_1$ from (8) are also shown in Table 3. In the homogeneous case, the subsidence is balanced by the divergence of the radiative flux and the divergence of the convective flux of the quantity $s - Ll$. For the inhomogeneous case, the horizontal advection term is relatively large and tends to lower the inversion at a rate comparable with the vertical motion and radiative and convective terms. In this case the radiative and convective processes are of insufficient magnitude to balance the vertical velocity and horizontal advection at the same height as for the homogeneous case. Since the subsidence rate in this model increases with height, a locally steady state solution can only be acheived at a lower level than the corresponding homogeneous case.

The rate terms for the equations predicting the slopes of q and s (eqs. 5 and 6) are shown in Table 3. In the steady-state homogeneous case the stabilization due to the large-scale subsidence is balanced by the convective destabilization. The destabilization associated with non-precipitating convection was discussed by Betts (1973). The radiative destabilization at cloud top deepens the layer directly, as does the convective flux divergence. The advection term in the inhomogeneous case has little effect on the stability.

The subsidence tends to increase the slope of q in the cloud layer. This is balanced by convective processes in the homogeneous case and by advection and convection in the inhomogeneous case as the slope of q decreases in the downstream direction.

Although the differences between the horizontally homogeneous case and the downstream solutions are small in the subcloud layer, these differences are important in explaining observed sea-surface temperature differences. The sea-surface temperature differences obtained for the homogeneous solutions are shown in Fig. 5 with the corresponding differences for the downstream solutions. For the homogeneous solutions, the temperature difference is approximately zero. For the advective case, however, the difference varies between 0.5 and 0.9 °C, which is consistent with the air–sea temperature generally observed in the trades (Hastenrath, 1977; Riehl et al., 1951). Consequently, the advection of cold air plays a major role in maintaining a small but positive heat flux at the surface. The moisture flux, however, is large and positive for both cases and will maintain a positive virtual heat flux even if the surface heat flux is zero. Advection does not significantly alter the moisture flux, although it does cause the boundary layer to be drier than the corresponding steady-state solutions.

The air–sea mixing ratio and temprature differences shown in Fig. 5 may be greater than is generally observed at warmer sea-surface temperatures. The relatively dry boundary layer associated with these solutions may result from the neglect of precipitation, which can evaporate in the subcloud layer, and the assumption of constant humidity and temperature profiles above the inversion, which in actuality can vary in the down stream direction. The effect of variations in the thermodynamic structure above the inversion on

Table 3. *Contributions of convective, advective, and radiative processes to the maintenance of locally steady-state solutions for horizontally homogeneous and inhomogeneous solutions at sea-surface temperatures of 26 °C*

	Horizontally homogeneous			Horizontally inhomogeneous			
	Convection	Vertical advection	Radiation	Convection	Vertical advection	Horizontal advection	Radiation
$\frac{1}{c_p}\frac{\partial s_M}{\partial t}$ (°C day^{-1})	1.50	0.00	−1.5	2.60	0.00	−1.10	−1.50
$\frac{\partial q_M}{\partial t}$ (g kg^{-1} day^{-1})	0.00	0.00	—	0.13	0.00	−0.13	—
$\frac{1}{c_p}\frac{\partial s_A}{\partial t}$ (°C day^{-1})	0.72	0.78	−1.50	1.84	0.74	−1.08	−1.50
$\frac{\partial q_A}{\partial t}$ (g kg^{-1} day^{-1})	1.36	−1.36	—	0.78	−0.82	−0.04	—
$\frac{\partial \gamma_s}{\partial t}$ (kJ kg^{-1} mb^{-1} day^{-1})	−0.0061	0.0061	—	−0.0079	0.0072	0.0007	
$\frac{\partial \gamma_q}{\partial t}$ (g kg^{-1} mb^{-1} day^{-1})	0.0105	−0.0105	—	0.0047	−0.0079	0.0032	—
$\frac{\partial p_I}{\partial t}$ (mb day^{-1})	30.3	76.8	46.5	45.5	−55.9	−31.1	41.5

the boundary layer structure is considered later in this section.

The results shown in Fig. 4 also reflect the rate at which the structure responds to variations in sea-surface temperatures since V is held constant during the integrations. Thus, at a given temperature, a downstream solution obtained with β_T = 4 °C (1000 km)$^{-1}$ has reached that temperature in half the time that the β_T = 2 °C (1000 km)$^{-1}$ solution requires. The steady-state solutions correspond to the $t = \infty$ solution.

From Fig. 4 it is apparent that the mixed layer temperature and moisture respond relatively quickly to changes in the boundary conditions, while changes in the inversion height occur at a slower rate. In the limit as β_T approaches large values, the downstream structure will differ little from the initial conditions at a given sea-surface temperature. For variations in the height of the inversion this limit is approached for relatively small values of β_T, while for the structure below the inversion, the limit is approached at much higher values of β_T.

To illustrate the time dependence of the adjustment of the boundary layer to surface temperature variations, the model response to a 2 °C jump in surface temperature was studied. The mixed layer and inversion height variations are shown in Fig. 6. After 30 h the mixed layer temperature and moisture are nearly at their steady-state values. The inversion height, however, is still increasing at 60 h and does not reach steady-state until ~120 h. This response is consistent with the downstream variations studied by Schubert et al. (1979) using a stratocumulus model.

These results indicate that for large temperature gradients and strong winds, the initial conditions may be more important than the actual temperature gradients in determining the height of the inversion at a given point. For lower wind speeds, a similar argument holds, since, although a decrease in the wind speed increases the time required for air to move a given distance, the surface fluxes also decrease and the response of the system is slowed.

3.3. *Variations in large-scale divergence*

Downstream calculations with a constant sea-surface temperature and divergence decreasing with distance were made. The downstream variations in the height of the inversion for $\beta_D = -2$ and -4×10^{-6} s^{-1} (1000 km)$^{-1}$ are shown in Fig. 7. For both calculations the height of the transition

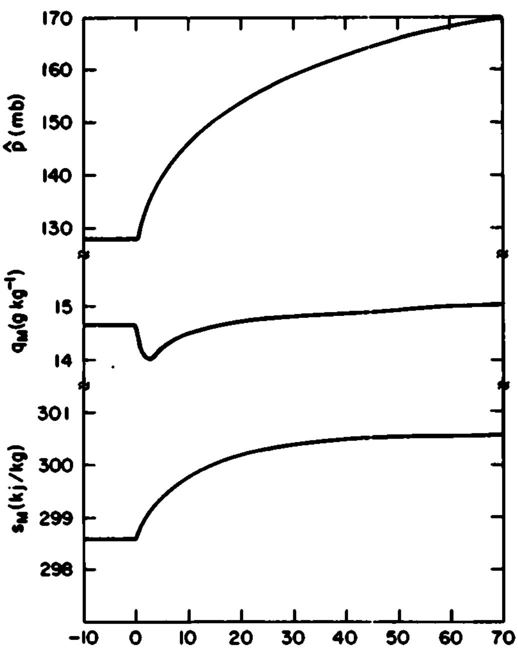

Fig. 6. Response of the model predicted inversion height and mixed layer dry static energy and mixing ratio to a 2 °C jump in surface temperature.

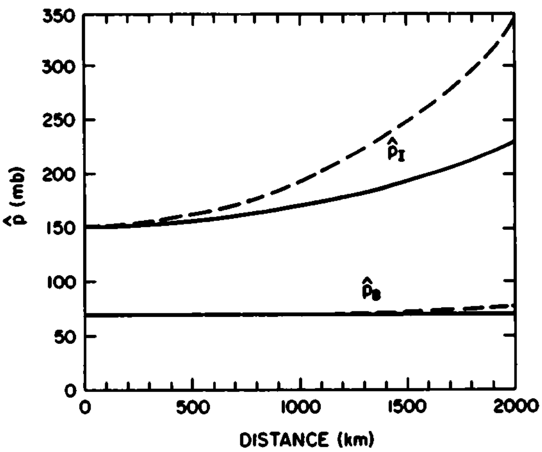

Fig. 7. Downstream variations in the inversion height and transition layer for divergence decreasing at the rate of $2 \times 10^{-6}\ s^{-1}/1000$ km (solid) and $4 \times 10^{-6}\ s^{-1}/1000$ km (dashed). Sea-surface temperature is constant.

layer shows little downstream variation. The height of the inversion, however, increases significantly in the downstream direction. The subcloud layer depth is defined by the LCL, which depends on the subcloud layer temperature and humidity. These quantities are also constant with distance as is shown in Fig. 8, where downstream variations in the thermodynamic structure below the inversion are shown for the $\beta_D = -2 \times 10^{-6}\ s^{-1}\ (1000\ km)^{-1}$. The insensitivity of the thermodynamic structure below the inversion to the specified divergence is consistent with the steady-state results presented in A79 and the results presented by Soong and Ogura (1979) using a model which explicitly considers the role of convective elements in modifying the temperature and moisture structure of the trade-wind boundary layer.

The height of the trade inversion obtained for horizontally homogeneous conditions is compared to the corresponding downstream solutions in Table 4. The inversion height for the homogeneous solutions is significantly greater than the solution obtained with divergence decreasing. However, the homogeneous solutions may be unrealistic in some

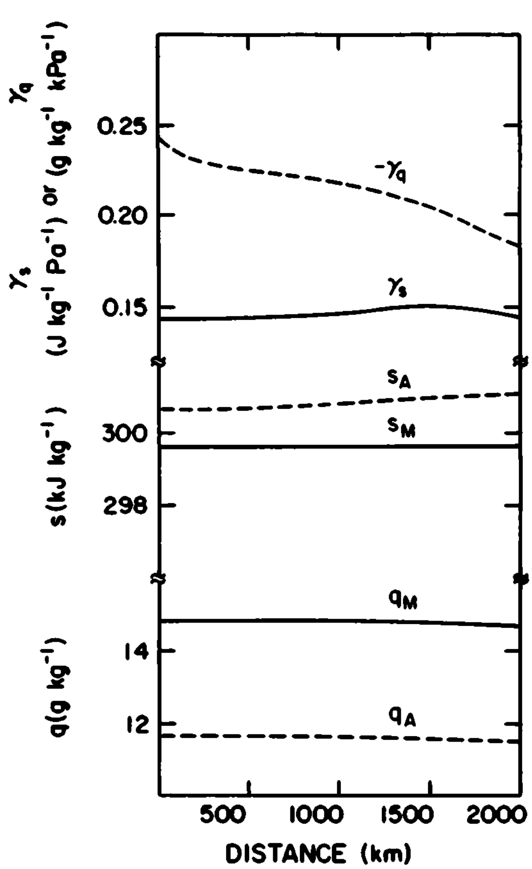

Fig. 8. Downstream variations in the thermodynamic structure below the inversion for $\partial D/\partial x = -2 \times 10^{-6}$ $s^{-1}/1000$ km and constant sea-surface temperature.

Table 4. *Comparison of inversion heights for horizontally homogeneous solutions, $\beta_D = -2 \times 10^{-6}\ s^{-1}$ (1000 km)$^{-1}$ and $\beta_D = -4 \times 10^{-6}\ s^{-1}$ (1000 km)$^{-1}$ with $D_I = 5 \times 10^{-6}\ s^{-1}$*

	$\hat{p}_I$ (mb)		
Divergence ($\times 10^{-6}\ s^{-1}$)	Horizontally homogeneous	$\beta_D = -2 \times 10^{-6}\ s^{-1}$ (1000 km)$^{-1}$	$\beta_D = -4 \times 10^{-6}\ s^{-1}$ (1000 km)$^{-1}$
2	389	196	177
3	260	173	163
4	196	158	155
5	153	153	153

cases since they have cloud layers of sufficient depth that the neglect of precipitation processes may be unrealistic. Furthermore, the temperature and moisture structure above the inversion may also change in the downstream direction which could alter the height of the inversion in both the homogeneous and inhomogeneous cases. In spite of these uncertainties, it is apparent that the time required for the inversion height to respond to variations in the large-scale divergence is large compared to the advective time scale. As a result, at a given location the height of the inversion may depend significantly on the past history of the inversion height and be influenced less by the instantaneous divergence.

The solutions obtained above were all obtained with V constant. This implies that the divergence results from a divergence of the trajectories, which may be the dominant effect in the trades, rather than variations in speed. The other extreme, with the divergence due solely to the speed divergence, is considered by assuming that $dV/dx = D_I + \beta_D x$. This equation is solved to give V as a function of x.

Solutions with V varying were obtained with $\beta_D = -2 \times 10^{-6}\ s^{-1}$ (1000 km)$^{-1}$ and $\beta_T = 2$ °C (1000 km)$^{-1}$ and were compared to solutions obtained with a fixed V. Downstream variations in the mixed layer dry static energy and mixing ratio and the inversion and transition layer heights are shown in Fig. 9. In the V varying case, V increases from 8.0 to ~14.0 m s^{-1} over 2000 km. The increase in V in the downstream direction results in a slightly warmer boundary layer due to increased surface fluxes. The inversion height, however, is not significantly different for the two cases shown. If D

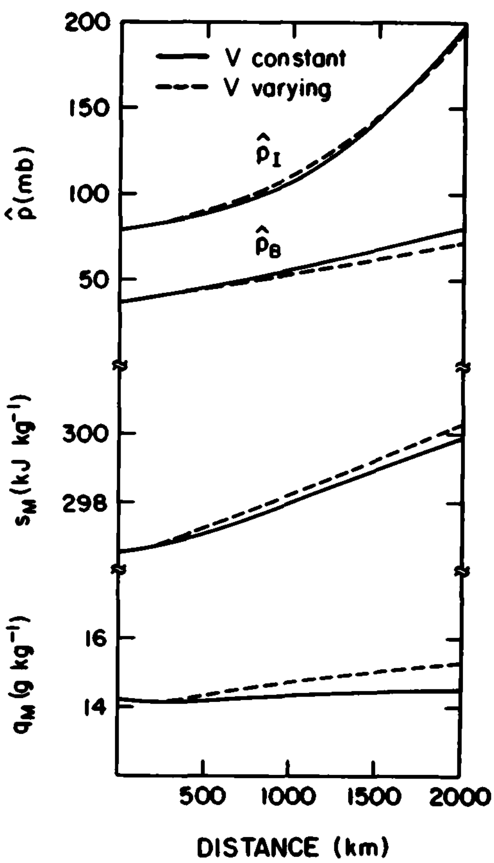

Fig. 9. Downstream variations in inversion height, transition layer height, subcloud layer dry static energy and mixing ratio with V constant and V increasing downstream ($\beta_T = 2$ °C (1000 km)$^{-1}$, $\beta_D = -2 \times 10^{-6}$ s^{-1} (1000 km)$^{-1}$).

is fixed at the value of 5×10^{-6} s^{-1}, which is the value used for the sea-surface temperature experiments, the variation in V in the x direction is larger and the effect on the structure is somewhat greater than that shown here.

3.4. *Other downstream effects*

Although the downstream variations in the thermodynamic structure of the trades is generally attributed to the increase in sea surface and the decrease in large-scale divergence, other effects may be important. For example, the temperature and moisture above the inversion generally increases in the downstream direction. Low-level cloud amounts can also vary significantly along a trajectory and these variations can affect the radiative fluxes.

The sensitivity of downstream solutions to variations in the thermodynamic structure above the inversion was illustrated. For these calculations, $\beta_T = 2$ °C (1000 km)$^{-1}$ and $\beta_D = -2 \times 10^{-6}$ s^{-1} (1000 km)$^{-1}$. Downstream increases in s_{00}, the intercept in (19), of 3 kJ kg^{-1} (1000 km)$^{-1}$ and an increase in q_{00} of 2.5 g kg^{-1} (1000 km)$^{-1}$ were assumed. These values are chosen for illustration purposes only and represent relatively significant downstream variations in the structure above the inversion. These results for this case are compared to the results obtained with constant boundary conditions in Fig. 10.

The assumed downstream variations of the upper boundary have some important effects. Increasing the dry static energy above the inversion maintains a relatively strong inversion which results in lower inversion heights. At 2000 km, the inversion height for the solution with a variable upper boundary is 50 mb lower than the reference case. There is, however, a stronger convergence of moisture below the inversion since the moisture discontinuity at the inversion decreases and less moisture convergence at the inversion is required to maintain the lower inversion. Consequently, the boundary layer moistens. At 2000 km downstream the mixed layer is ~2 g kg^{-1} moister than the reference case. The subcloud layer, however, is only slightly warmer than the reference solution. The transition layer height for the variable upper boundary case is nearly constant, and results from the downstream increase in the mixing ratio and the increase in dry static energy.

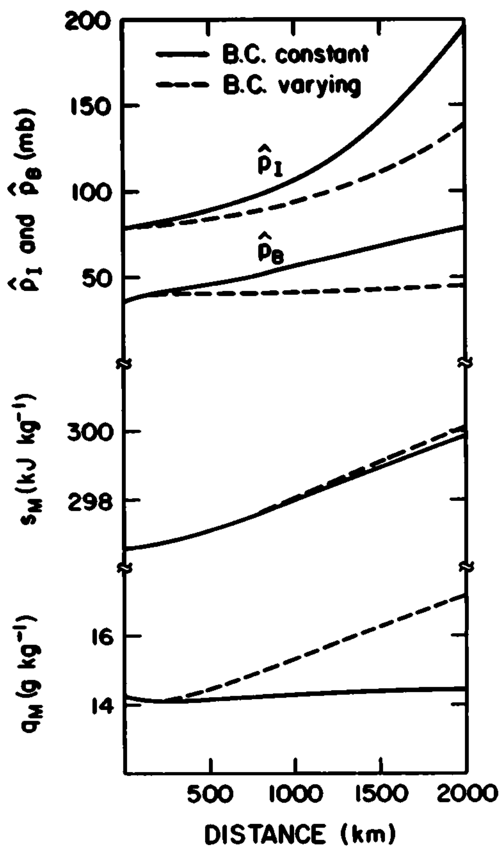

Fig. 10. Downstream variation in the inversion height, transition layer height, subcloud layer dry static energy and mixing ratio with the thermodynamic structure above the inversion constant and with structure above the inversion varying.

The subcloud layer differences discussed above have a significant effect on the air-sea differences in temperature and humidity. The differences for these solutions are shown in Fig. 5. The other downstream solutions shown in this figure were obtained with $\beta_D = 0$. The divergence, however, has little effect on these differences. Consequently, the differences between the two downstream solutions shown in Fig. 5 are principally due to downstream variations in the structure above the inversion. The solution with varying upper boundary conditions shows a nearly constant air-sea difference in mixing ratio compared to the significant increase in this difference as sea-surface temperature increases.

Although radiative effects are fixed for the downstream solutions shown above, radiative effects may also change downstream. No attempt is made to include these effects interactively since the radiation effects should not be externally specified, but should be obtained from the temperature, moisture, and cloud structure both in and above the boundary layer.

Downstream solutions were obtained, however, with different values assigned to the total longwave cooling. For the cases presented above, the longwave cooling averaged over the entire boundary layer is 3 °C day^{-1}. Calculations were also made with average cooling rates of 2 and 4 °C day^{-1} for $\beta_T = 2$ °C (1000 km)$^{-1}$ and $\beta_D = -2 \times 10^{-6}$ s^{-1} (1000 km)$^{-1}$. The downstream variations in the model parameters for these cases were compared to the case where the total cooling is 3 °C/day^{-1}. The downstream variations in the inversion height were most sensitive to the specification of the radiative cooling. The downstream variation in the inversion height for a cooling rate of 4 °C day^{-1} was ~30 mb greater than the corresponding downstream difference obtained with a cooling rate of 3 °C day^{-1}. The solution obtained with a cooling rate of 2 °C day^{-1} gave a downstream difference in the inversion height that was ~10 mb less than the reference case. Downstream variations below the inversion were relatively insensitive to the assumed cooling rate.

4. Conclusions

The trade-wind boundary layer is modeled as a layered structure consisting of a subcloud layer, transition layer, cloud layer, and trade inversion layer. The time and space variation of this structure is described using heat and moisture budget equations. Cumulus effects associated with non-precipitating cumulus clouds are parameterized using a simple scheme. This model is used to calculate variations in the thermodynamic structure of the trades due to downstream variations in externally specified parameters in the model.

The solutions obtained with sea-surface temperature increasing were compared with solutions obtained for horizontally homogeneous conditions. At a given sea-surface temperature, the advective solutions give a structure below the inversion that does not vary significantly from the corresponding homogeneous solution. The heat and moisture budgets for the downstream and the homogeneous solutions were compared. Although the advection terms in the heat budget were large, they are generally balanced by an increased convective heating relative to the steady-state solutions. This balance can be obtained without the subcloud layer temperature varying significantly from the sea-surface temperature. Although the variations in the boundary layer temperature and moisture due to downstream increases in the sea-surface temperature are small, the air–sea temperature differences are more realistic than those obtained with steady-state solutions.

Downstream variations in the temperature of the boundary layer are relatively insensitive to variations in surface wind speed, large-scale divergence, and the thermodynamic structure above the inversion. The variations in mixing ratio, however, are sensitive to downstream variations in the surface wind speed and the thermodynamic structure above the inversion.

Solutions obtained with a constant sea-surface temperature and divergence decreasing downstream show little variation in the structure below the inversion since heat and moisture budgets below the inversion are relatively insensitive to the vertical velocity. The downstream solutions in this case, however, show an inversion height which may be significantly less than the corresponding homogeneous height. The downstream variations in inversion heights are also relatively sensitive to downstream increases in sea-surface temperature and variations in the thermodynamic structure above the inversion. In these cases, as well as the case where divergence decreases, advection results in lower inversion heights, since $-V\,\partial \hat{P}_I/\partial x$ is less than zero and relatively large. It is apparent from these calculations that the inversion height may depend more significantly on the past history of the inversion than the local conditions.

The model results were obtained with a simple parameterization of the radiative fluxes. However, since the downstream integration occurs over days, the downstream solutions were found to be sensitive to the specification of the radiative fluxes. These results indicate that a realistic representation of the boundary layer requires that the radiative fluxes be parameterized as a function of the boundary layer cloudiness and the temperature and moisture structure above and within the boundary layer.

The calculated downstream variations of inversion heights are consistent with the observational results of Riehl et al. (1951). The Riehl et al. results were for a situation where the sea-surface temperature gradient was approximately 2 °C (1000 km)$^{-1}$, and although it was not calculated, divergence was most likely decreasing downstream. Their results indicate a downstream increase in the inversion height corresponding to variations in the pressure level of the inversion of approximately 50 mb (1000 km)$^{-1}$; cloud base increased slightly downstream. The model results clearly show that horizontally homogeneous conditions would give a significantly greater downstream variation in the inversion height than is observed.

Riehl et al. (1951) showed that the trades play an important role in the Hadley circulation through the accumulation of latent heat. The accumulated heat maintains deep convection near the equator. From the results presented above, it is apparent that the total water content of the lowest layers depends significantly on the height of the trade inversion. However, as was noted, the inversion height obtained for homogeneous conditions may vary significantly from the corresponding nonhomogeneous solutions, and may depend on initial conditions. Although the traditional view has been that the downstream variation of the thermodynamic structure of the trades is due to the downstream increase in sea-surface temperature and the decrease in large-scale divergence, the variations in the thermodynamic structure above the inversion may also be important. A more complete study of downstream variations could be made by incorporating this model into a general circulation model. Large-scale variables needed for the solutions would then be obtained from the large-scale model and would not have to be specified externally.

5. Acknowledgements

I would like to thank Karen Palen for typing this manuscript. A major portion of this work was performed at the Pennsylvania State University and was funded by the Global Atmospheric Research Program, Division of the Atmospheric Sciences, National Science Foundation, and the GATE Project Office, National Oceanic and Atmospheric Administration under Grant ATM78-98715 and ATM80-09307.

REFERENCES

Albrecht, B. A. 1979. A model of the thermodynamic structure of the trade-wind boundary layer: Part II. Applications. *J. Atmos. Sci. 36*, 90–98.

Albrecht, B. A. 1981. Parameterization of trade-cumulus cloud amounts. *J. Atmos. Sci. 38*, 97–105.

Albrecht, B. A., Betts, A. K., Schubert, W. H. and Cox, S. K. 1979. A model of the thermodynamic structure of the trade-wind boundary layer: Part I. Theoretical formulation and sensitivity tests. *J. Atmos. Sci. 36*, 73–89.

Augstein, A., Reihl, H., Ostapoff, F. and Wagner, V. 1973. Mass and energy transports in an undisturbed Atlantic trade wind flow. *Mon. Wea. Rev. 101*, 101–111.

Augstein, A. and Wendel, M. 1980. Modelling of the time-dependent atmospheric trade-wind boundary layer with non-precipitating cumulus clouds. *Contrib. Atmos. Phys. 53*, 509–538.

Betts, A. K. 1973. Non-precipitating cumulus convection and its parameterization. *Q. J. R. Meteorol. Soc. 86*, 178–196.

Betts, A. K. 1975. Parametric interpretation of trade-wind cumulus budget studies. *J. Atmos. Sci. 32*, 1934–1945.

Cho, H.-R. 1977. Contribution of cumulus life-cycle effects to the large-scale heat and moisture budgets. *J. Atmos. Sci. 34*, 87–97.

Fitzjarrald, D. R. and Garstang, M. 1981. Vertical structure of the tropical boundary layer. *Mon. Wea. Rev. 109*, 1512–1526.

Fraedrich, K. 1974. Dynamic and thermodynamic aspects of the parameterization of cumulus convection: Part II. *J. Atmos. Sci. 31*, 1838–1849.

Hastenrath, S. and Lamb, P. J. 1977. *Climatic atlas of the tropical Atlantic and eastern Pacific Oceans.* University of Wisc. Press. 97 pp.

Holland, J. and Rasmusson, E. 1973. Measurements of the atmospheric mass, energy, and momentum budgets over a 500-kilometer square of tropical ocean. *Mon. Wea. Rev. 101*, 44–55.

Kraus, E. B. and Leslie, L. D. 1982. The interactive evolution of the oceanic and atmospheric boundary layers in the source regions of the trades, *J. Atmos. Sci. 39*, 2760–2772.

LeMone, M. A. and Pennell, W. T. 1976. The relationship of trade wind cumulus distribution to subcloud layer fluxes and structure. *Mon. Wea. Rev. 104*, 524–539.

Lilly, D. K. 1968. Models of cloud-topped mixed layers under a strong inversion. *Q. J. R. Meteorol. Soc. 94*, 292–309.

Mak, M. K. 1976. A study of the downstream variation of the lower trade-wind circulation. *Tellus 28*, 97–107.

Malkus, J. S. 1956. On the maintenance of the trade winds. *Tellus 8*, 335–350.

Nicholls, S. and LeMone M. A. 1980. The fair weather boundary layer in GATE: The relationship of subcloud fluxes and structure to the distribution and enhancement of cumulus clouds. *J. Atmos. Sci. 37*, 2051–2067.

Nitta, T. and Esbensen, S. 1974. Heat and moisture budgets using BOMEX data. *Mon. Wea. Rev. 102*, 17–28.

Ogura, Y. 1977. A note on the downstream variation of the lower trade-wind circulation. *Tellus 29*, 240–244.

Riehl, H., Yeh, T. C., Malkus, J. S. and La Seur, N. E. 1951. The northeast trade of the Pacific Ocean. *Q. J. R. Meteorol. Soc. 72*, 598–626.

Riehl, H. and Malkus, J. S. 1957. On the heat balance and maintenance of circulation in the trades. *Q. J. R. Meteorol. Soc. 83*, 21–28.

Schubert, W. H., Steiner, E. J. and Cox, S. K. 1979. Marine stratocumulus convection, Part II. Horizontally inhomogeneous solutions. *J. Atmos. Sci. 36*, 1308–1324.

Sommeria, G. 1976. Three dimensional simulation of turbulent processes in the undisturbed trade wind boundary layer. *J. Atmos. Sci. 33*, 216–241.

Soong, S.-T. and Ogura, Y. 1980. Response of trade-wind cumuli to large-scale processes. *J. Atmos. Sci. 37*, 2035–2050.

Stull, R. B. 1976. The energetics of entrainment across a density interface. *J. Atmos. Sci. 33*, 1260–1267.